

**OPEN ACCESS**

## Rapid Thermal Processed $\text{CuInSe}_2$ Layers Prepared by Electrochemical Route for Photovoltaic Applications

To cite this article: Ashwini B. Rohom *et al* 2018 *J. Electrochem. Soc.* **165** H3051

View the [article online](#) for updates and enhancements.

### You may also like

- [Electrical and photovoltaic characteristics of  \$\text{CuInSe}\_2\$  thin films processed by nontoxic Cu-In precursor solutions](#)  
Ik Jin Choi, Jin Woo Jang, Seung Min Lee et al.
- [Unravelling the intricacies of selenization in sequentially evaporated  \$\text{Cu\(In,Ga\)Se}\_2\$  Thin film solar cells on flexible substrates](#)  
G Regmi, Sangita Rijal and S Velumani
- [A robust approach to fabricate CZTSSe absorber layer for solar cells via a self-selenizations process conducted by concentrated selenium solution](#)  
Xiaojie Yuan, Shuwen Xue, Jun Liao et al.



### Your Lab in a Box!

The PAT-Tester-i-16: All you need for Battery Material Testing.

- ✓ All-in-One Solution with integrated Temperature Chamber!
- ✓ Cableless Connection for Battery Test Cells!
- ✓ Fully featured Multichannel Potentiostat / Galvanostat / EIS!

[www.el-cell.com](http://www.el-cell.com) +49 40 79012-734 [sales@el-cell.com](mailto:sales@el-cell.com)

**EL-CELL**<sup>®</sup>  
electrochemical test equipment





## Rapid Thermal Processed CuInSe<sub>2</sub> Layers Prepared by Electrochemical Route for Photovoltaic Applications

Ashwini B. Rohom, Priyanka U. Londhe, and Nandu B. Chaur<sup>z</sup>

Electrochemical Laboratory, Department of Physics, Savitribai Phule Pune University, Pune, Maharashtra 411007, India

Impact of rapid thermal (RT) annealing and normal selenization process on the properties of CuInSe<sub>2</sub> (CIS) layers prepared by electrochemical route is reported. Cyclic voltammetric measurement was carried out to optimize the co-deposition potentials. A range of characterization techniques were employed to study the properties. Three prominent reflections (112), (204/220) and (312/116) of tetragonal CIS were exhibited in as-deposited CIS layers. Upon selenization, the crystallinity was found to be improved. Uniform, compact, densely packed surface morphology was observed in as-prepared sample. Large grains are developed upon RT annealing due to recrystallization. Elemental composition obtained by EDAX confirms the growth of stoichiometric layers. Photo-electrochemical study demonstrates the p-type conductivity. Current-voltage, capacitance-voltage, electrochemical impedance spectroscopy were conducted to investigate the influence of the grain size and crystallinity on electrical properties. Energy band-gap estimated from absorption spectra were 1.18, 1.04 and 0.98 eV for as-deposited, selenized, RT annealed samples, respectively. X-ray Photoelectron spectroscopy confirms the presence of Cu<sup>+</sup>, In<sup>3+</sup> and Se<sup>2-</sup> oxidation states in all CIS layers. Power conversion efficiency of 3.05% and 5.94% were achieved for selenized and RT annealed samples, respectively. The improved efficiency measured for RT annealed sample is proposed due to the growth of highly crystalline, large grain and compact surface morphology.

© The Author(s) 2017. Published by ECS. This is an open access article distributed under the terms of the Creative Commons Attribution Non-Commercial No Derivatives 4.0 License (CC BY-NC-ND, <http://creativecommons.org/licenses/by-nc-nd/4.0/>), which permits non-commercial reuse, distribution, and reproduction in any medium, provided the original work is not changed in any way and is properly cited. For permission for commercial reuse, please email: [oa@electrochem.org](mailto:oa@electrochem.org). [DOI: 10.1149/2.0081804jes] All rights reserved.



Manuscript submitted August 31, 2017; revised manuscript received November 17, 2017. Published December 8, 2017. *This paper is part of the JES Focus Issue on Processes at the Semiconductor-Solution Interface.*

Considering the energy crisis, solar energy has emerged as an important non-conventional energy source. Various direct bandgap, high optical absorption coefficient materials have been used toward the fabrication of thin film solar cells. CuInSe<sub>2</sub>(CIS) is one of the intensively studied active absorber materials in solar cells because of its direct bandgap  $\sim 1.05$  eV, high absorption coefficient, large mean free path and long diffusion length of minority carriers.<sup>1,2</sup> Furthermore, the energy gap can be increased upon addition of gallium and/or sulfurization in controlled ambient. Device efficiency over 22% has been achieved for CIGS based thin film solar cells using co-evaporation method.<sup>3</sup> However, in spite of high efficiency the high production cost is one of these severe obstacles. Various reports are available in the literature on the development of CIS solar cells using vacuum<sup>4</sup> and non-vacuum processes.<sup>5</sup> Electrochemical technique has been used for the preparation of CIS based solar cells.<sup>6</sup> A low-cost electrochemical technique is widely used for the growth of metal oxide, insulator and semiconductor thin films because of higher growth rate, deposition over arbitrary shaped surface, possibility to grow highly crystalline and controlled stoichiometric alloy thin films. The best reported CIGS solar cells produced via this technique have measured 15.4% efficiency by Bhattacharya et al.<sup>7</sup> in conjunction with PVD method. Electrodeposition of CIS thin films can be performed either by one-step<sup>8</sup> or two-step approach.<sup>9</sup> Fabrication of CIS solar cells from aqueous<sup>10</sup> as well as non aqueous electrolyte<sup>11</sup> is also reported.

There are many challenging opportunities in optimizing thin film properties by using graded band-gap<sup>12</sup> and nanoparticles based<sup>13</sup> absorber layers. Post-deposition treatments such as surface etching and annealing are needed to improve the performance of solar cells.<sup>14,15</sup> Several reports are available on annealing treatments performed in vacuum or in inert gas atmosphere leads to improvement in crystallinity of the as-grown layer.<sup>16</sup>

Herein, we report the fabrication of CIS thin films using one-step electrodeposition and subsequent post deposition annealing. Annealing process is carried out with two different procedures. In the first approach as-prepared CIS layers were selenized with elemental Se in tubular furnace and another approach was rapid thermal annealing

(RTP). In the first approach selenization can be performed under selenium atmosphere at high temperature. Selenium atmosphere can be made via elemental Se vapor<sup>17</sup> or H<sub>2</sub>Se/Ar at atmospheric pressure.<sup>18</sup> However, safety concerns have to be taken into account in case of H<sub>2</sub>Se gas therefore in spite of H<sub>2</sub>Se gas Se vapors thermally generated from solid precursor were used. Furthermore, RTP annealing was performed in order to reduce the Se loss in self formed film without additional Se vapor or H<sub>2</sub>Se. In this article we have demonstrated the effect of above annealing ways on properties of electrodeposited CIS layer as well as on the solar characteristics.

### Experimental

**Chemicals.**—All chemicals used for the deposition of CIS layers were purchased from Sigma-Aldrich of purity at least 99.9%. Fluorine doped tin oxide (FTO) coated glass substrates of sheet resistance  $\sim 10$ – $15 \Omega/\text{cm}^2$  were purchased from Pilkington Glass Company, UK. The double distilled deionized water (DDDW) was used as a solvent.

**Electrodeposition of CIS layers.**—Electrodeposition of CIS thin film was carried out potentiostatically using  $\mu 3$ AUT 70762 AUTO-LAB potentiostat/galvanostat with three-electrode assembly consists Ag/AgCl, graphite plate and FTO as reference, counter and working electrodes, respectively. The initial characterizations associated to the quality of layer were studied for the sample electrodeposited onto FTO substrate, whereas the solar cells were prepared by depositing CIS onto FTO/CdS substrate. The FTO substrates were ultrasonically cleaned with acetone and rinsed in DDDW. The electrolyte matrix, 3 mM copper chloride (CuCl<sub>2</sub>), 6 mM indium chloride (InCl<sub>3</sub>) and 3 mM selenous acid (H<sub>2</sub>Se<sub>2</sub>O<sub>3</sub>) with pH hydron buffer (pH 3) solution was used to deposit CIS layers. Lithium chloride (LiCl) was used as a supporting electrolyte. Cyclic voltammetry measurement was performed to optimize the co-deposition potential for Cu, In and Se. CIS layers were deposited at  $-0.8$  V with respect to Ag/AgCl without agitation at room temperature. Immediately after deposition the samples were thoroughly rinsed in DDDW and dried in an ambient condition.

**Electrochemical measurements.**—The cyclic voltammetry and chronoamperometric measurements were performed using  $\mu 3$ AUT

<sup>z</sup>E-mail: [n.chaure@physics.unipune.ac.in](mailto:n.chaure@physics.unipune.ac.in)

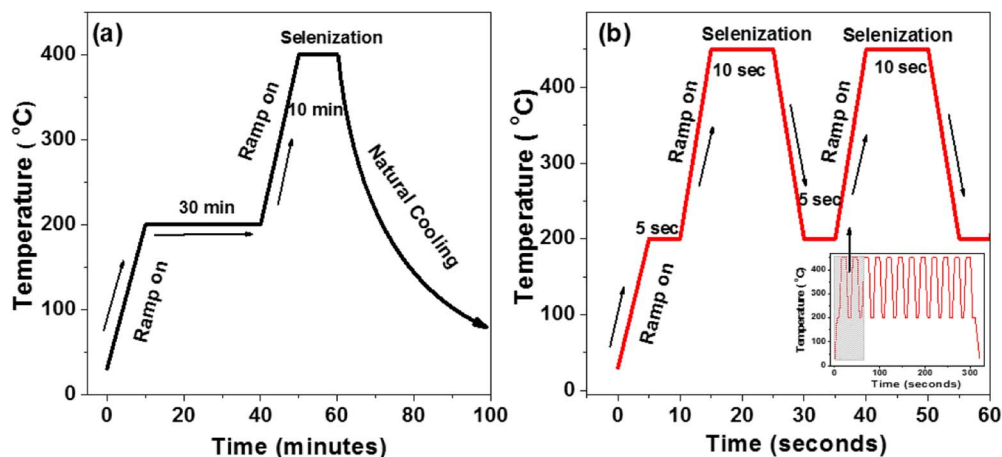


**Figure 1.** Schematic for variation of annealing temperature with time in a) selenization and b) RTP process used in the post deposition treatment for CIS thin films.

70762 AUTOLAB potentiostat/galvanostat. A conductivity type of the sample was obtained using photoelectrochemical (PEC) measurements. A three-electrode geometry consisting graphite, Ag/AgCl and CIS layer as counter, reference and working electrodes, respectively were used in 1 M KCl solution. A white light source of intensity 10 mW/cm<sup>2</sup> was used to illuminate the samples. Impedance spectroscopy was studied with Biologic SP 300 potentiostat for frequency range 1 MHz to 100 mHz in 1 M NaCl solution. A similar setup employed for PEC was used to study the impedance spectroscopy.

**Materials characterization.**—The structural properties were studied by means of X-ray diffractometer, model Bruker D8 with Cu K $\alpha$  anode of wavelength 0.154 nm. Optical absorption measurements were performed with JASCO V-770 UV-vis-NIR spectrophotometer. Surface morphology was examined by using scanning electron microscope (SEM) model JEOL JSM 6360 A. A thin layer (~20 nm) of platinum was sputtered on the surface of sample prior to record SEM images. Atomic percentage concentration was determined by energy dispersive X-ray analysis (EDAX) technique attached with SEM unit. Biologic SP 300 Potentiostat equipped with two probe measurement setup was employed to study the electrical properties. Invia Renishaw micro Raman spectrophotometer, with an excitation laser of wavelength 785 nm was employed to study the detail structural properties. The elemental composition and chemical states were analyzed using X-ray Photoelectron Spectroscopy PHI 5000 Versa Probe II instrument equipped with a monochromatic X-ray source, Al K $\alpha$  of energy 1486.6 eV and hemispherical analyzer. A solar stimulator with power intensity 100 mW/cm<sup>2</sup> was used to study the optoelectronic properties of the solar cell.

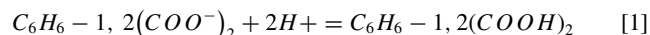
**Post-deposition annealing treatments.**—A two different approaches were employed to anneal the CIS layers, first, a two-step selenization with elemental Se vapors and secondly, rapid thermal annealing process. In the two-step selenization process the chamber was initially heated to 200°C for 30 minutes and subsequently the temperature was raised to 450°C with ramp rate 5°C/s for 10 minutes. The samples were cooled naturally to room temperature. RTP system (MTI Corporation, USA) was used to anneal the sample in argon ambient. Initially, the temperature was raised to 200°C at the rate 30°C/s and maintained for 5 sec. The temperature was further increased to 450°C and maintained for 10 sec. The sample was cooled rapidly with rate 50°C/s to 200°C. The RTP process was repeated for 10 cycles. Figures 1a and 1b shows the schematic of two-step selenization process and RTP, respectively. A full program used for RTP annealing is given in inset of Figure 1b.

**Fabrication of solar cells.**—A superstrate device structures, glass/FTO/CdS/selenized CIS/metal (Au) and glass/FTO/CdS/RTP

annealed CIS/metal were prepared to study the optoelectronic properties. CdS thin layers of thickness ~50 to 70 nm were grown onto FTO by chemical bath deposition technique.<sup>19</sup> The annealed CIS layers were etched in Br-CH<sub>3</sub>OH solution and subsequently in NaCN solution to remove the unwanted secondary phases. Finally, a circular Au contacts of diameter ~3 mm were made using thermal evaporator at pressure ~5 × 10<sup>-5</sup> mbar.

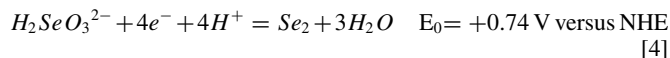
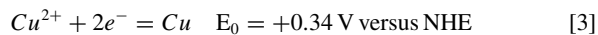
## Results and Discussion

**Cyclic voltammetry and chronoamperometry.**—The electrochemical behavior of Cu, In and Se was investigated using the cyclic voltammetric measurement. A typical cyclic voltammogram (CV) recorded in presence of Cu, In and Se ions with hydron buffer 3 solution<sup>20-22</sup> at 5 mV/sec scan rate is depicted in Figure 2a. The hydron pH 3 buffer solution is a mixture of 0.15 wt% sulfamic acid and 0.30 wt% potassium bipthalate, used to reduce the free H<sup>+</sup> and OH<sup>-</sup> ions present in the electrolyte according to the following reactions,

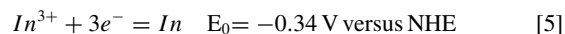


The potassium compound from pH 3 hydron buffer and LiCl was used to enhance the ionic conductivity of an electrolyte.

The cyclic voltammetry study for CIS and CIGS was reported previously.<sup>23</sup> The features noticed in the cathodic scan upto -0.4 V are assigned to the reduction of Cu and Se by the following charge-transfer reactions,

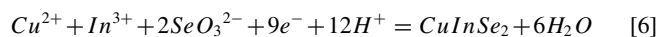


An elemental In is proposed to be electrodeposited in the region above -0.55 V by the charge transfer reaction;



The plateau region attributed about -0.5 V to -0.85 V assigned to the diffusion controlled growth which is proposed to be suitable for the synthesis of stoichiometric CIS layers. The sharp rise in the current observed around -0.95 V is associated to the over potential deposition of metallic In and/or the In-rich CuInSe<sub>2</sub> thin layer.

The formation of CIS is proposed by the following half-electrode reaction,



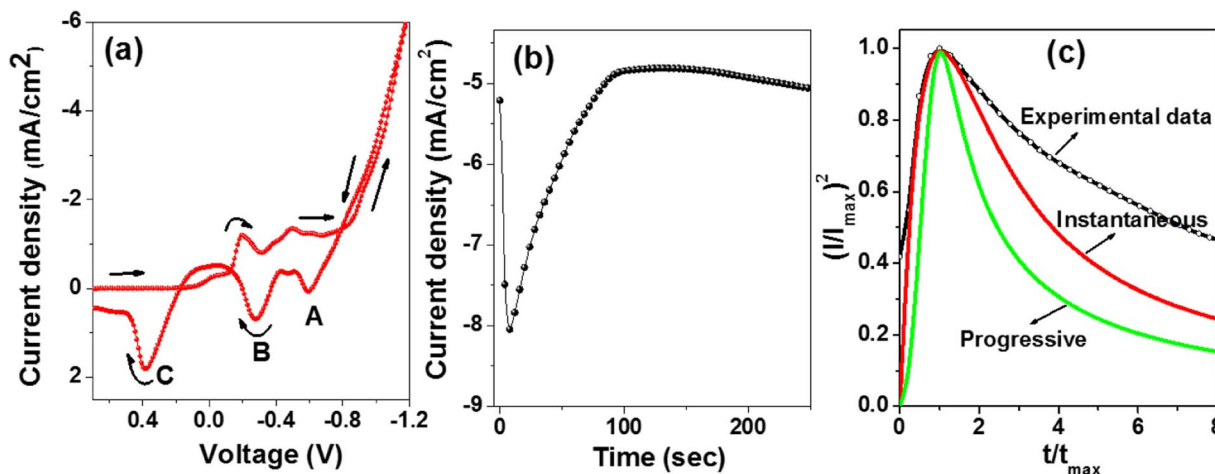


**Figure 2.** a) Cyclic voltammogram of CIS solution recorded at 5 mV/Sec with respect to Ag/AgCl reference electrode, b) chronoamperometric curve for potentiostatic deposition of CIS at  $-0.8$  V and c) current-time transient plots of  $(I/I_{\max})^2$  versus  $(t/t_{\max})^2$  for the study of the nucleation and growth mechanism during the electrodeposition of CIS.

The anodic curve is represented by reverse arrows in Figure 2. The peaks 'a', 'b', and 'c' appeared at  $-0.58$  V,  $-0.27$  V and  $0.38$  V are proposed due to the oxidation of In-rich, Cu-rich and Se-rich phases of CIS, respectively. In our previous report we have clearly demonstrated that the films grown at higher cathodic potential  $-0.9$  V and  $-1.0$  V are In-rich and the presence of indium selenide related peaks were clearly seen in the XRD spectra.<sup>8</sup> The layers deposited at  $-0.8$  V versus Ag/AgCl reference were found to be close to stoichiometric and highly crystalline, therefore the effect of selenization and RTP annealing was investigated on this layer.

The chronoamperometric, current-time transient curve measured for the layer obtained at  $-0.8$  V is depicted in Figure 2b.

The steady-state current is given by,

$$I = 4nDFcA \quad [7]$$

where, 'D' is the diffusion coefficient, 'A' is the area, 'c' is the concentration, 'F' is the Faraday constant and 'n' is the number of electrons transferred per molecule. The rapid decay observed initially is proposed due to the charging/discharging of double layer.<sup>24</sup>

The nucleation mechanism was studied from the chronoamperometric data fitted into Scharifker and Hills model which shows the electroactive species mass transport.<sup>25</sup>

The following equations can be used to describe the instantaneous and progressive nucleation,

For instantaneous nucleation,

$$\left(\frac{I}{I_m}\right)^2 = 1.9542 \left(\frac{t}{t_m}\right) - 1 \times \left\{1 - \exp\left[-1.2564 \left(\frac{t}{t_m}\right)\right]\right\}^2 \quad [8]$$

$$\left(\frac{I}{I_m}\right)^2 = 1.2254 \left(\frac{t}{t_m}\right) - 1 \times \left\{1 - \exp\left[-2.3367 \left(\frac{t}{t_m}\right)\right]\right\}^2 \quad [9]$$

Figure 2c depicts the  $(I/I_{\max})^2$  versus  $(t/t_{\max})^2$  plot of experimental and theoretical data obtained from Equations 8 and 9. It is observed that the experimental data agreeing well with instantaneous nucleation obtained by Scharifker and Hills model. This suggests that all reaction sites on surface are simultaneously activated and during the initial stage of deposition the numbers of nuclei on surface are saturated.

**Structural analysis: XRD and raman studies.**—Structural investigation of as-grown, selenized and RTP processed CIS layers studied by X-ray diffractometer are shown in Figure 3. Three prominent reflections (112), (204/220) and (116/312) correspond to tetragonal structure of CIS are exhibited at about  $26.30^\circ$ ,  $44.30^\circ$  and  $51.52^\circ$ ,

respectively. The peaks attributed due to FTO substrate are marked as solid circle (●). Highly crystalline CIS layers without secondary phases were obtained upon selenization and RTP annealing. The degree of enhancement in the crystallinity was studied by the full width at half maxima (FWHM) and the average crystallite size by Debye-Scherrer formula.<sup>26</sup> The calculated values of FWHM and average crystallite size are summarized in Table I. Upon selenization, the FWHM and average crystallite size were decreased due to recrystallization of material.

RTP process was found to be more effective to increase the crystallinity and grain growth probably due to the rapid cooling of sample. During recrystallization the strain may develop in the layer, which is determined by Williamson-Hall (W-H) equation,<sup>27</sup>

$$\beta \cos \theta = \eta \sin \theta + \frac{\lambda}{t} \quad [10]$$

where, ' $\beta$ ' is the FWHM of diffraction peaks, ' $\theta$ ' is the Bragg diffraction angle, ' $\lambda$ ' is the wavelength of X-ray source ' $\eta$ ' is the strain and ' $t$ ' is the average crystallite size. The plots of  $\beta \cos \theta$  versus  $\sin \theta$  for

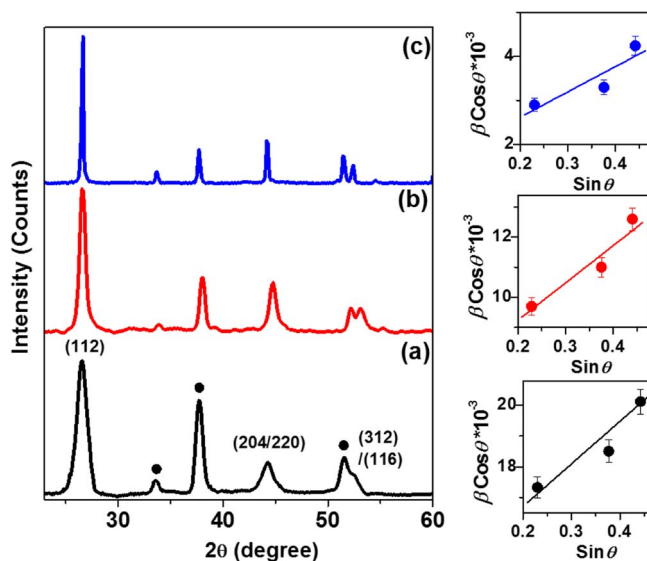


**Figure 3.** XRD pattern of as-prepared a), selenized b) and RTP annealed c) CIS layer electrodeposited at  $-0.8$  V. The corresponding plots of  $\beta \cos \theta$  versus  $\sin \theta$  are given in inset of each XRD pattern.

**Table I.** A summary of crystallite size and strain calculated by the Hall equation and Scherrer formula obtained from XRD results for as-prepared, selenized and RTP annealed CIS layers.

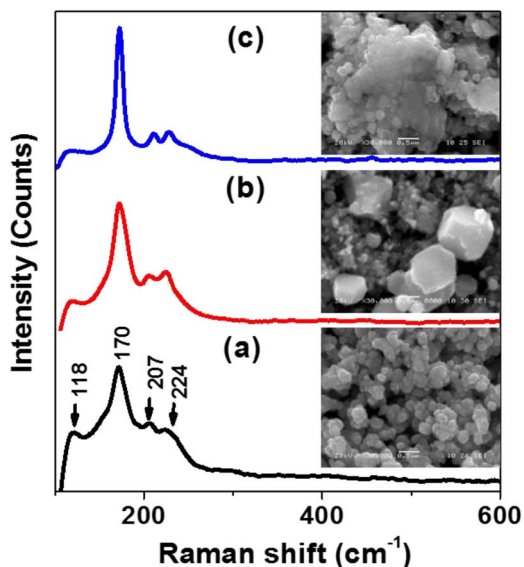
CIS film deposited at $-0.8$ V	Average FWHM of all peaks (degrees)	Crystallite size (nm) from Debye Scherer formula	Williamson-Hull analysis		
			Crystallite size (nm)	Types of strain (Tensile 'T' or Compressive 'C')	Strain $\times 10^{-3}$
As-deposited	1.159	10.13 nm	11.53 nm	T	5.738
Selenized	0.6896	17.77 nm	23.38 nm	T	11.89
RTP annealed	0.2152	44.71 nm	56.98 nm	T	13.86

all samples are given in the inset of respective XRD spectra. The average crystallite size obtained from W-H analysis is in good agreement with the values obtained from Scherrer analyses. The positive value of strain reveals the presence of tensile strain in the crystal lattice.<sup>28</sup>

Nonetheless, the XRD pattern alone is insufficient to identify the phase purity of sample. In order to understand the more structural details, the Raman spectroscopy was used. The Raman spectra of as-prepared a), selenized b) and RTP annealed c) samples electrodeposited at  $-0.8$  V is shown in Figure 4. A strong peak attributed about  $170\text{ cm}^{-1}$  corresponds to A1 mode of chalcopyrite CIS phase.<sup>29</sup> The peaks exhibited about  $207\text{ cm}^{-1}$  and  $224\text{ cm}^{-1}$  are corresponds to E and B2 modes of CIS phase. The broadening of the most intense band (A1 mode) was found to be decreased for RTP annealed sample is proposed due to the enhancement in the degree of crystallinity and reduced defects. The features related to secondary phases or ODC were not observed in Raman spectra.<sup>30-31</sup> The peak appeared at  $118\text{ cm}^{-1}$  in all samples corresponds to the laser line which generally use for the calibration of Raman wave number.

**Surface properties and compositional analysis: SEM and EDAX.**—SEM micrographs of as-prepared, selenized and RTP annealed CIS layers grown at  $-0.8$  V is given in inset of Figure 4. The as-prepared layers exhibited granular morphology having particle size  $\sim 500$  nm. Upon selenization a large clusters of size 2 micron can be clearly seen by the agglomeration of small grains. However, the RTP annealed sample resembles a well faceted large island like particles. A significant change in the surface morphology of RTP annealed sample can be clearly seen in SEM picture.

The bulk composition of CIS layer was obtained by EDAX analyses. The as-grown layers were Se-deficient whereas a nearly stoichio-

**Figure 4.** Raman spectra of a) as-prepared, b) selenized and c) RTP annealed CIS layers. Inset shows the corresponding SEM micrographs magnified at  $0.5\ \mu\text{m}$  scale.**Table II.** A summary of EDAX results obtained for as-prepared, selenized and RTP annealed CIS layers electrochemically grown at  $-0.8$  V versus Ag/AgCl reference electrode.

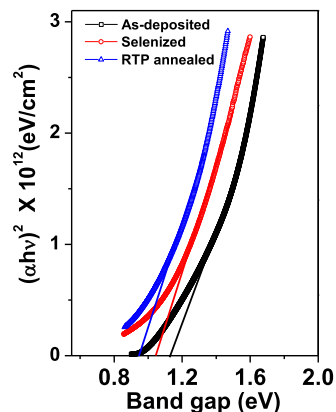
CIS electrodeposited at $-0.8$ V	Atomic composition in percentage		
	As-deposited	Selenized	RTP annealed
Copper (Cu)	27.39	29.08	29.90
Indium (In)	28.92	19.43	21.35
Selenium (Se)	43.70	50.58	48.75
Se/Cu	0.78	1.04	0.94

metric sample was deposited upon selenization and RTP annealing. All layers were Cu-rich. The atomic percentage concentrations obtained by EDAX analysis is summarized in Table II. The result obtained by EDAX agrees well with the XRD and Raman results.

**Optical properties.**—Figure 5A shows the  $(\alpha h\nu)^2$  versus  $h\nu$  plot of as-prepared, selenized and RTP annealed CIS layers. The values of the energy bandgap, 1.18, 1.04 and 0.98 eV were estimated by extrapolating the straight region of the curve. The large band-gap observed for as-grown layer could be associated to the growth of off-stoichiometric precursor layers and the growth of non-uniform particles.

The decreased bandgap measured upon selenization and RTP annealing could be due to the enhancement in particles as well as the recrystallization of material. The bandgap estimated for RTP annealed layer is in good agreement with the reported value.<sup>32</sup> Note that, the lack of sharp fundamental absorption edges for all plots can be associated to the multiple reflections that take place at the surface and grain boundaries and slight variation in the particle size.<sup>33</sup>

**Photo-electrochemical properties.**—The conductivity type of the layer was studied by knowing the majority charge carriers with PEC analysis. The photoresponse curve recorded upon illumination with

**Figure 5.** Optical absorption spectra,  $(\alpha h\nu)^2$  versus  $h\nu$  of as-prepared, selenized and RTP annealed CIS layers prepared at  $-0.8$  V.

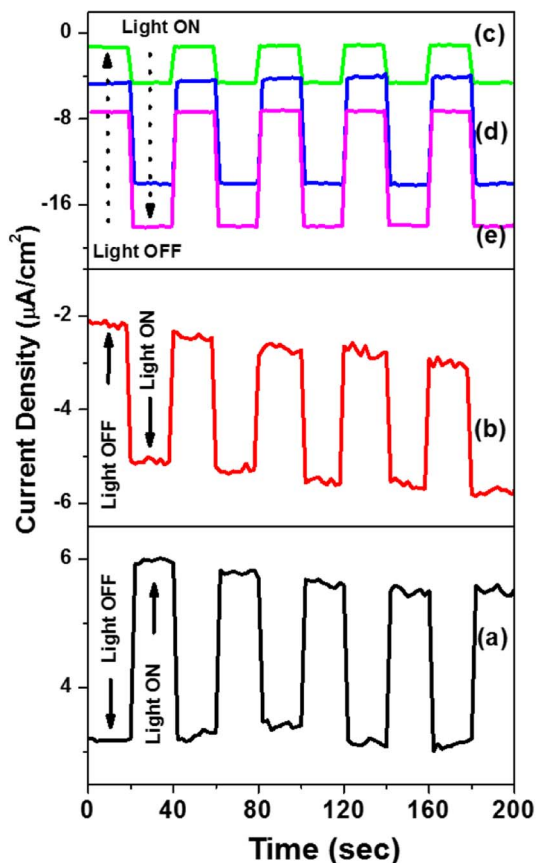


**Figure 6.** Photo response curves, photocurrent density versus time for standard n-type silicon a), p-type silicon b), as-prepared c), selenized d) and RTP annealed e) CIS layers.

chopped white light is shown in Figure 6. The measured photocurrent response was compared with standard n and p-type Si samples of resistivity 0.5  $\Omega$ -cm a) and b), respectively.

The photocurrent originates from the minority carriers, therefore, the direction of observed photocurrent can give type of majority charge carriers. The photocurrent measured for n-type sample upon illumination was increased toward the positive direction (Figure 6a), whereas, the enhancement in the photocurrent was noticed along the negative direction for p-type Si sample (Figure 6b). From PEC studies the growth of p-type conductivity layer was inferred.<sup>34</sup>

The p-type behavior observed in as-deposited CIS thin films can be ascribed to intrinsic defects such as selenium vacancies or binary phases related to  $\text{In}_x\text{Se}_y$ . A small applied negative bias could extract the electrons from the conduction band, therefore the electrons in the conduction band of p-type semiconductor are negligible. However, upon illumination the transportation of electrons from the valence band to the conduction band takes place, which could further driven to the solid/electrolyte interface and finally transferred to the solution by reduction of the  $\text{H}^+$  ions results an enhancement in the cathodic current.<sup>35</sup> Along with this, the photocurrent observed to be increased for RTP annealed samples. This fact may be associated with the improved crystallinity and particle size of CIS. The sharp edges observed during ON and OFF of the light indicates the selenized CIS layer may have less defects and could be suitable for the development of high efficiency thin film solar cells.

**Electrical properties (J-V and C-V).**—To explore the electrical properties J-V and C-V measurements have been studied. Au metal contacts of diameter 3 mm were made on CIS layer by thermal evaporation technique. The semilogarithmic plots,  $\ln(I)$  versus applied bias (V) for as-prepared, selenized and RTP annealed CIS layers are de-

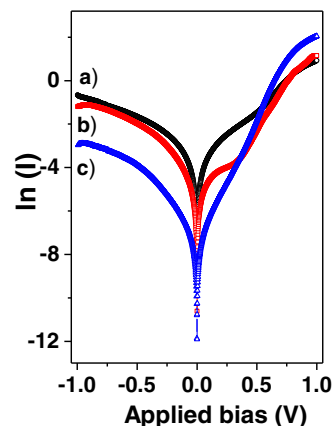


**Figure 7.** Semilogarithmic graphs,  $\ln(I)$  versus applied bias (V) for as-prepared a), selenized b) and RTP annealed c) CIS layers.

picted in Figure 7. The values of the ideality factor, 'n' is calculated from the slope of the straight line region for forward bias using the following equation,<sup>36</sup>

$$n = \frac{q}{kT} \frac{dV}{d(\ln I)} \quad [11]$$

where  $q$ ,  $V$ ,  $n$ ,  $k$ ,  $T$  and  $I$  are the charge of electron, applied bias, ideality factor, Boltzmann constant, temperature and diode current, respectively. The 'n' values, 1.73, 1.15 and 1.04 were calculated for as-prepared, selenized and RTP annealed CIS layers, respectively. The higher value of 'n' for as-deposited CIS layers could be associated to the leakage current at the metal-semiconductor interface or defect level presents within the material or at the interface. The value of 'n' calculated for RTP annealed sample is close to unity (ideal diode condition) is proposed due to the enhancement in the electronic properties of CIS. The reverse current measured for as-grown sample is due to the structural disorders, such as grain boundaries which may provide a high resistive path for the transfer of charge carriers.

The flatband potential and carrier concentration was determined by Mott-Schottky (M-S) plot. Figure 8 shows the M-S ( $1/C^2$  versus applied bias) plots of as-prepared a), selenized b) and RTP annealed c) CIS layers. The negative slope indicates the p-type conductivity.<sup>37</sup> Three distinct regions, namely inversion, depletion and accumulation are clearly seen in Figure 8. The flatband potentials 0.75, 0.64 and 0.47 V were estimated for as-prepared, selenized and RTP annealed CIS layers, respectively. The variation in the flatband potential is the sign of the variation of the band edge position which is shown to depend on the oxidation state of the surface. The more oxidized surface gives the more positive the band edge position. The slope of M-S plots were further used to calculate the carrier concentration by using the expression,<sup>38</sup>

$$1/C^2 = \frac{2}{q\epsilon_s A^2 N} (V_{bi} - V) \quad [12]$$

Where  $V_{bi}$  is the flatband potential and  $N$  is the charge carrier concentration.

The carrier concentrations  $1.17 \times 10^{16}$ ,  $2.02 \times 10^{18}$ ,  $2.51 \times 10^{19}$   $\text{cm}^{-3}$  were calculated for as-prepared, selenized and RTP annealed samples, respectively. The increased carrier concentration for RTP annealed sample is associated to the increases crystallinity and reduction in grain boundaries which is desirable for the development of high efficiency thin film solar cell. The calculated values of flatband potentials, carrier concentrations and ideality factor are summarized in Table III.

**Electrochemical impedance spectroscopy [EIS] analysis.**—EIS was performed to investigate the characteristic features of the samples. Figure 9a shows the Nyquist plots, complex plane real  $|Z'|$  versus

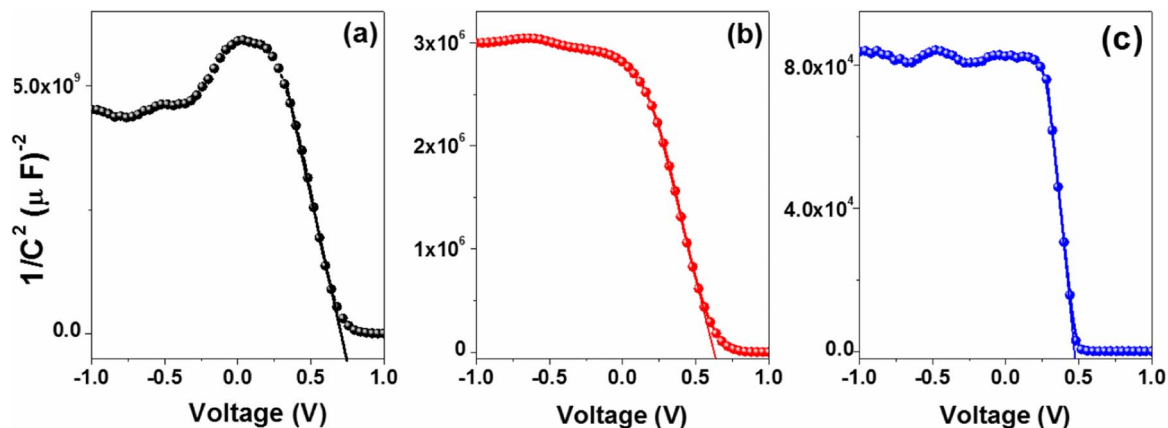


**Figure 8.** Mott Schottky plots ( $1/C^2$  versus Voltage) for as-prepared a), selenized b) and RTP processed c) CIS layers recorded for frequency 100 KHz.

**Table III.** Flat band potential and carrier concentration values calculated from capacitance-voltage measurement for as-prepared, selenized and RTP annealed CIS layers.

CIS film deposited at $-0.8$ V	Flat band potential (V)	Carrier concentration ( $/\text{cm}^3$ )	Ideality factor
As-deposited	0.748	$1.17 \times 10^{16}$	1.73
Selenized	0.637	$2.02 \times 10^{18}$	1.15
RTP annealed	0.468	$2.51 \times 10^{19}$	1.04

imaginary  $|Z''|$  impedance, obtained for the frequencies 1 MHz–0.1 mHz for as-deposited, selenized and RTP annealed CIS samples. The straight line at low frequency is proposed to be due to the diffusion process of electroactive species known as Warburg impedance ( $Z_w$ ). The values of series resistance associated to the electrolyte ( $R_s$ ), the charge transfer resistance ( $R_{ct}$ ), the capacitance of electrical double layer ( $C_d$ ) at the solid-electrolyte interface, and  $Z_w$  can be calculated by fitting the data into equivalent circuit. The equivalent circuit is given in Figure 9b. The estimated values of above parameters are summarized in Table IV. Since the ionic diffusion and heterogeneous charge transfer occur as successive mechanism, therefore the

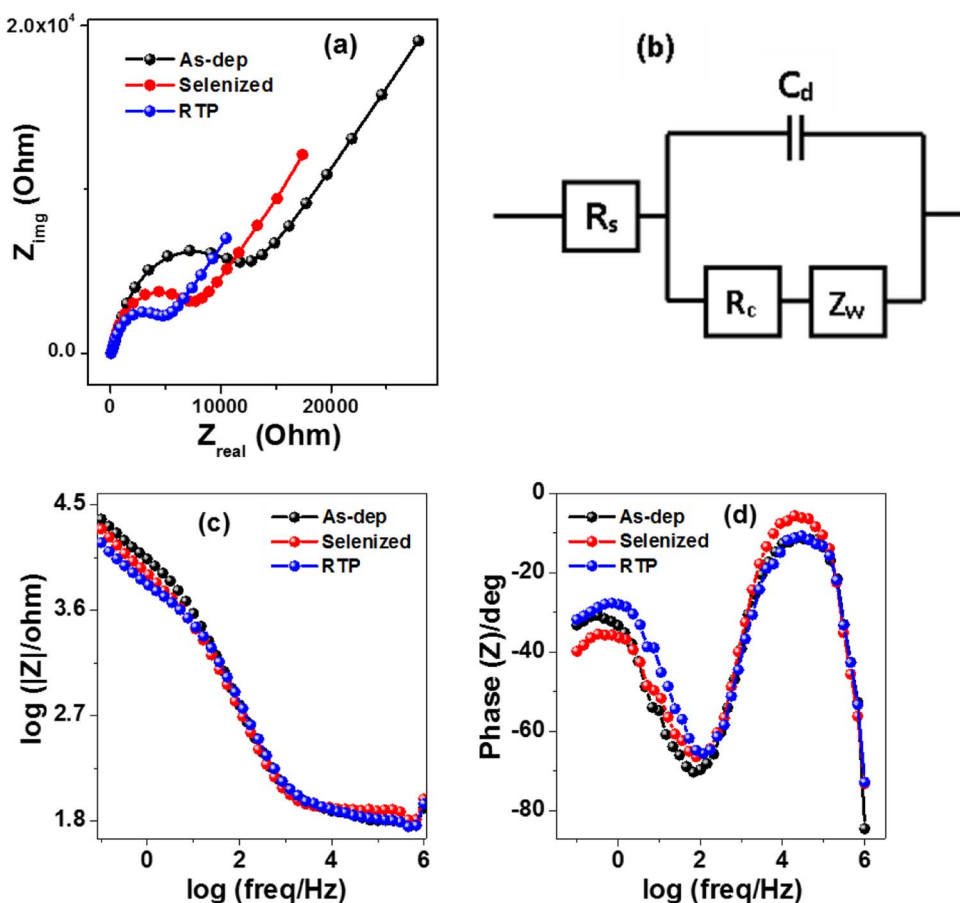


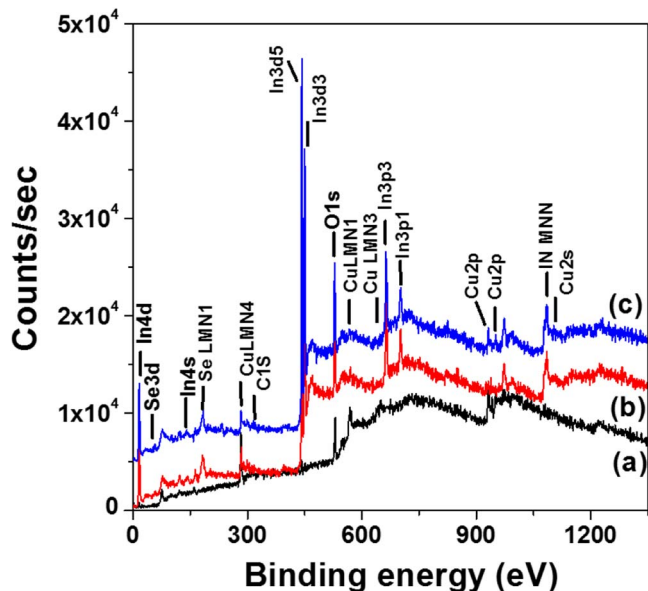
**Figure 9.** (a) Nyquist plot, (b) Equivalent circuit model used, (c) and (d) Bode plots of the as-deposited, selenized and RTP annealed CIS thin films.

**Table IV.** Best fit values of  $R_s$ ,  $R_{ct}$ ,  $C_d$  and  $Z_w$  using an equivalent circuit for as-prepared, selenized and RTP annealed CIS layers.

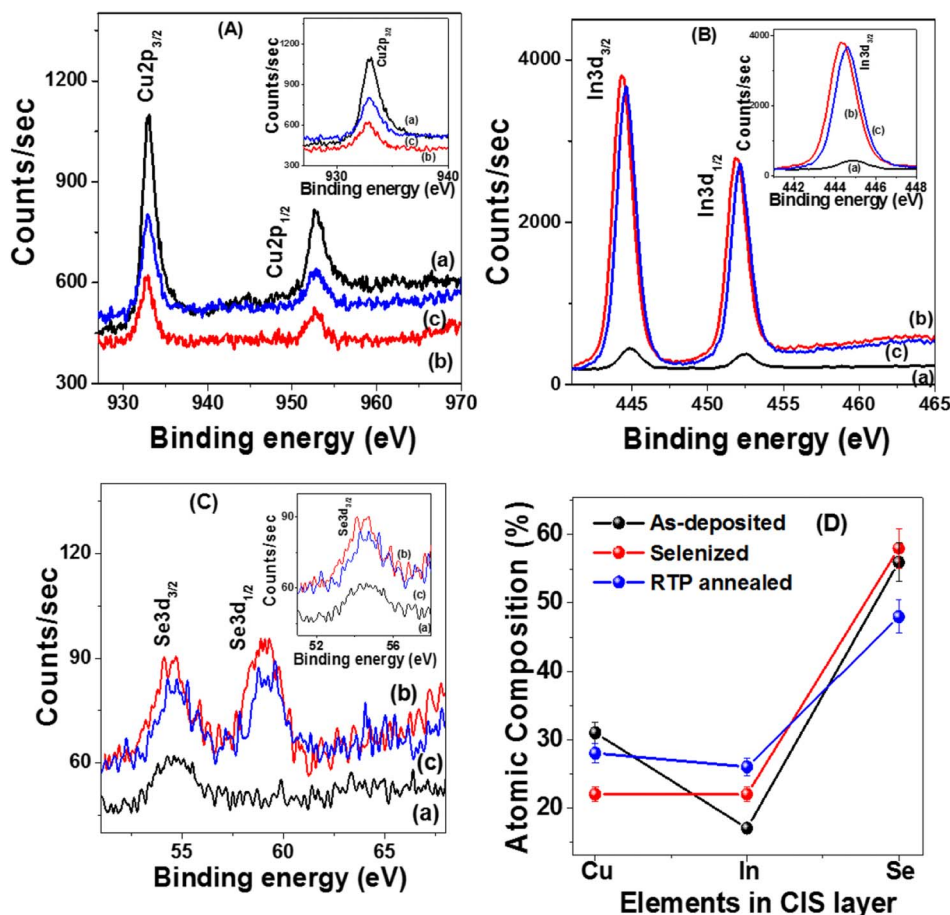
CIS film deposited at $-0.8$ V	$R_s$ ( $\Omega$ )	$R_{ct}$ ( $\Omega$ )	$C_d$ ( $\mu\text{F}$ )	$Z_w$ ( $\Omega$ )
As-deposited	41.25	8897	0.3	6986
Selenized	54.36	3476	5.0	5531
RTP annealed	47.70	2575	6.8	4763

equivalent circuit is composed of  $Z_w$  and  $R_s$ . It is known that the  $Z_w$  depends on the applied frequency.<sup>39</sup> No significant changes in the values of  $R_s$  were observed for these samples. The values of  $R_{ct}$  were found to be systematically decreased for selenized and RTP annealed CIS layer as compared with as-deposited CIS samples is proposed to be due to the decreased grain boundaries. The RTP annealed CIS film exhibits a considerably larger value of  $C_d$  compared to both as-deposited and selenized CIS thin films. Basically, an electric double layer exists at the interface between the electrode and its surrounding electrolyte, therefore, the charged electrode is separated by an insulated space with electrolyte which forms a capacitor.  $C_d$  is nothing but amount of charge accumulated in this double layer. The increased value of  $C_d$  could be due to the higher conductivity of recrystallized CIS layer. Figures 9c and 9d shows the Bode plots ( $\log |Z'|$  versus  $\log$  (frequency) and phase-angle versus  $\log$  (frequency)) obtained in the frequencies 1 MHz-0.1mHz. The corresponding peak position of negative phase-angle is shifted toward higher frequency range for RTP annealed CIS layer, reveals a higher electrical capacitance value.<sup>40</sup>

**X-ray photoelectron spectroscopy analysis.**—The composition and oxidative states of CIS layers are investigated using XPS analyses. Appropriate electrical charge compensation was employed to perform the analysis and binding energy for C 1s peak was referenced at 284.80

**Figure 10.** Survey scans of a) as-prepared, b) selenized and c) RTP annealed CIS layers.

eV. Figure 10 shows the survey spectrum for as-prepared, selenized and RTP annealed CIS layers. All survey spectra indicates the presence of copper, indium and selenium. Peaks related to C and O due to surface contamination are also observed. The core level spectrum for Cu, In and Se are examined and depicted in Figure 11. The Cu

**Figure 11.** Core level spectrum for A) copper, B) indium, C) selenium and D) atomic percentage concentration for Cu, In and Se in CIS layers.

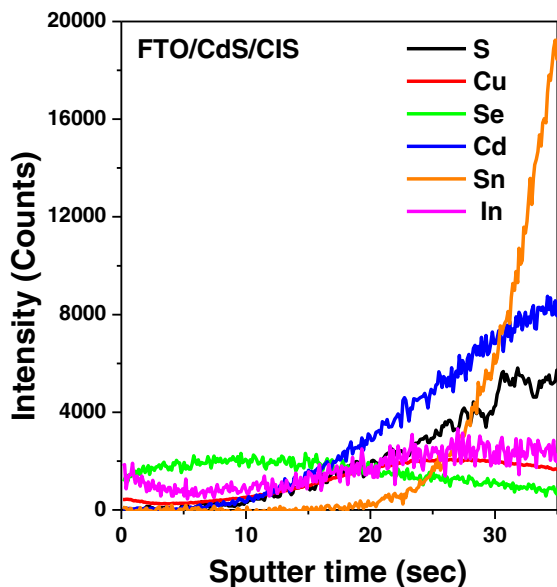


**Figure 12.** SIMS depth profile for individual atomic percentage concentration for Cu, In, Se, Cd, S and Sn in FTO/CdS/CIS structured thin film.

2p core level split into  $2p_{3/2}$  (932.99 eV) and  $2p_{1/2}$  (952.81 eV) peaks (Figure 11A) demonstrate the Cu valence state in CIS is +1.

Similarly, core level spectrum of In 3d split into two peaks  $3d_{5/2}$  (444.88 eV) and  $3d_{3/2}$  (451.96 eV) confirms the valence state of In in CIS to be +3 (Figure 11B). The core spectrum of the Se has doublet peaks of Se  $3d_{3/2}$  (54.71 eV) and Se  $3d_{1/2}$  (59.06 eV) (Figure 11C).<sup>41</sup> The core level spectrums for Cu  $2p_{3/2}$ , In  $3d_{5/2}$  and Se  $3d_{3/2}$  are shown in inset of Figures 11A, 11B and 11C for as-deposited, selenized and RTP annealed CIS layers. The Cu  $2p_{3/2}$  peak for as-deposited sample appeared at 933.00 eV shifted to 932.68 eV and 932.90 eV for selenized and RTP annealed samples, respectively. Similarly In  $3d_{5/2}$  and Se  $3d_{3/2}$  peak for as-deposited sample appear at 444.88 eV and 54.71 eV which are shifted toward 444.33 eV and 54.35 eV for selenized and 444.63 eV and 54.61 eV for RTP annealed CIS layer, respectively. These shifts are proposed due to the difference between the oxidation states of Cu, In and Se present in the CIS layers. For selenized CIS layers it has been noted that the peak shifted to lower binding energy as compared to RTP annealed sample could be due to the presence of excess Se on the surface.<sup>42</sup> A typical atomic concentration obtained for all sample about 5 min sputtering is shown in Figure 11D). The quantification obtained for RTP annealed layer gives the stoichiometric CIS layer.

**Secondary ion mass spectroscopy (SIMS) analysis.**—The compositional study performed by SIMS measurements for RTP annealed sample as shown in Figure 12. SIMS measurements clearly demonstrated the Cd and S was not diffused into the CIS layer as the Cd and S was determined close to the substrate within  $\sim 70$  nm width. Further, a uniform growth of all the elements i.e. Cu, In and Se were observed for entire thickness of the layer.

**Solar cell characteristics.**—The solar cell parameters, open circuit voltage ( $V_{OC}$ ), short circuit current ( $J_{SC}$ ), fill factor (FF) and power conversion efficiency  $\eta$ , were measured for CdS/selenized-CIS/Au and CdS/RTPannealedCIS/Au heterostructures under  $100 \text{ mW/cm}^2$  illumination. Prior to Au-metal contact the heterostructure layers were etched chemically in bromine-methanol solution for 60 sec and subsequently in NaCN solution to remove the secondary oxides/compounds phases formed during the selenization/RTP processes. The typical dark and illuminated J-V, curves for CdS/selenized-CIS and CdS/RTP annealed CIS solar cell are depicted in Figures 13A and 13B), respectively.

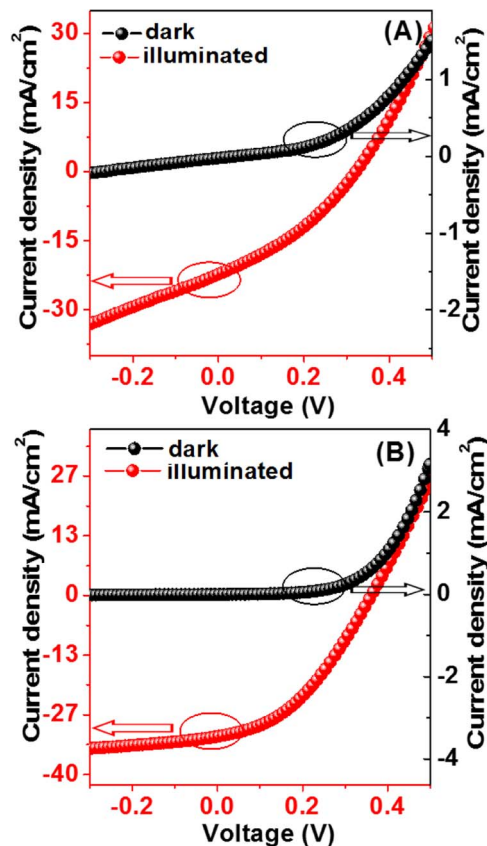


**Figure 13.** Dark and illuminated J-V characteristics for a typical superstrate configuration consisting of glass/FTO/CdS/selenized CIS /Au (A), and glass/FTO/CdS/RTP annealed CIS /Au, (B) heterostructure.

The power conversion efficiencies, 3.05% and 5.94% were measured for selenized and RTP annealed CIS layer, respectively. The increased efficiency measured for RTP annealed solar cell is proposed to be due to the increased particle size, degree of crystallinity and controlled stoichiometric composition of precursors.

The J-V behavior of a thin film solar cell (TFSC) can be described by a general single exponential diode equation as follows<sup>43</sup>

$$J = J_0 \exp \left[ \frac{q}{nkT} (V - R_s J) \right] + GV - J_L \quad [13]$$

where,  $J$  and  $V$  are the diode current density and applied bias voltage,  $J_0$  is the reverse saturation current density,  $J_L$  is the photocurrent density,  $R_s$  is the series resistance and  $G$  is the shunt conductance.

The derivative  $dV/dJ$  against  $1/J$  and  $dV/dJ$  against  $1/(J+J_{SC})$  for,  $R_s G \ll 1$  plotted to dark and illuminated condition using Equation 13) is shown in inset of Figures 14a, 14c and 14b, 14d, respectively.

$$\frac{dV}{dJ} = R_s + \left[ \frac{nkT}{q} (J + J_{SC})^{-1} \right] \quad [14]$$

The values of the series resistance,  $R_s$  determined from the intercept to y-axis for CdS/selenized-CIS/Au and CdS/RTPannealedCIS/Au heterostructure were  $50.41 \Omega\text{-cm}^2$ ,  $5.16 \Omega\text{-cm}^2$  and  $23.40 \Omega\text{-cm}^2$ ,  $4.31 \Omega\text{-cm}^2$  under dark and illuminated condition, respectively.

The values of shunt conductance,  $G$  were extracted by plotting  $dJ/dV$  versus  $V$  as shown in Figures 14a, 14c and 14b, 14d for dark and illuminated condition, respectively. The values of  $G$  were obtained from the minimum value of the slope  $dJ/dV$  in reverse bias. Shunt conductance of the fabricated device in dark and illuminated condition are  $0.9 \text{ mS/cm}^2$  and  $36.2 \text{ mS/cm}^2$  for CdS/selenized-CIS/Au and  $0.4 \text{ mS/cm}^2$  and  $7.5 \text{ mS/cm}^2$  for CdS/RTPannealedCIS/Au heterostructure respectively. For an efficient photovoltaic device the shunt conductance has to be as small as possible. Smaller value of  $G$

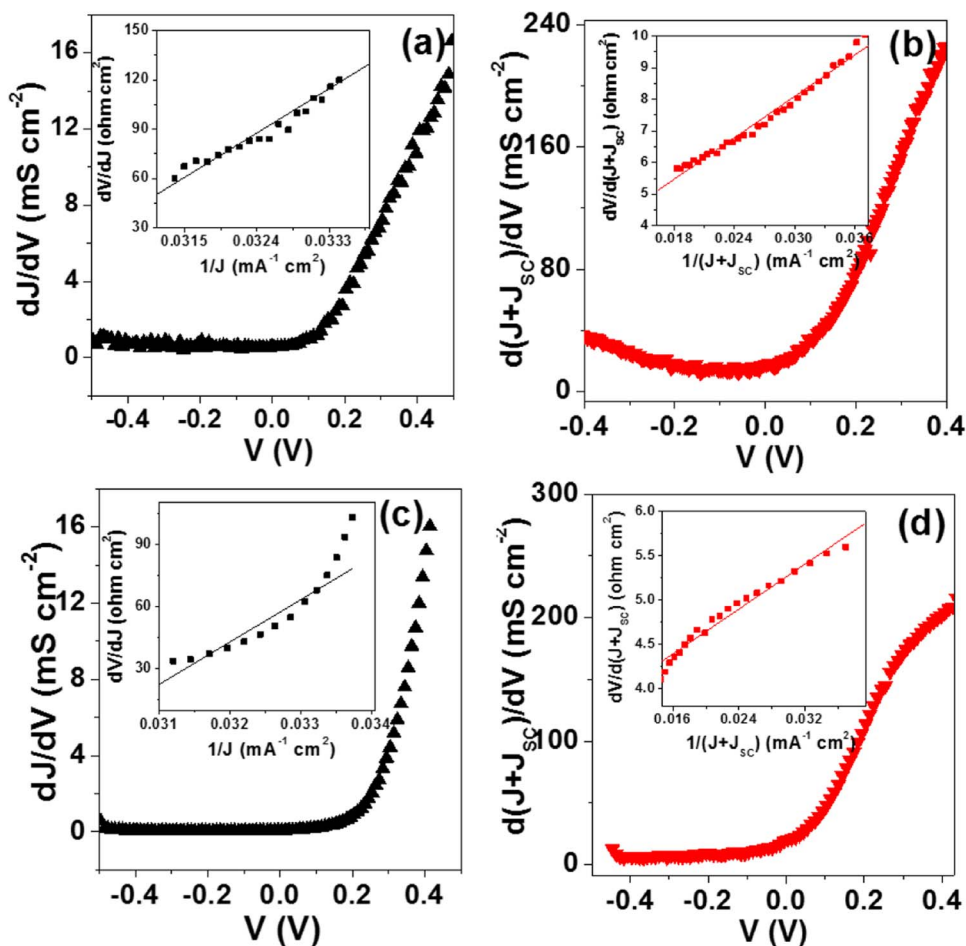


**Figure 14.** Plots of  $dJ/dV$  versus  $V$  (a, c) and  $d(J+J_{sc})/dV$  versus  $V$  (b, d) for glass/FTO/CdS/selenized CIS/Au and glass/FTO/CdS/RTP annealed CIS/Au heterostructure solar cell device measured under dark and illuminated conditions, respectively. The corresponding  $dV/dJ$  versus  $1/J$  in dark and  $dV/d(J+J_{sc})$  versus  $1/(J+J_{sc})$  under illumination are shown in inset of respective curves.

represents the less internal leakage through the cell. The results of the diode analysis for the  $J-V$  data under illumination are summarized in Table V.

As it is noted that the type of annealing affects on the several properties of layer which further improve the power conversion efficiency (PCE). The device made from selenized CIS shows less PCE than the RTP annealed CIS layer. One of the possible reason can be the shorter processing time of the RTP process, which not only resulted in the improved quality of absorber layer but which can avoid the growth of detrimental phases in the absorber layer. High degree of shunting is observed in the devices made from selenized CIS layer which could be due to the porous nature of the film compared with the RTP annealed CIS layer which forms compact layer. However, comparing literature for a device with the present results, the best PCE value obtained for RTP annealed layer is less which could be due to the large density of inter grain trap states in CIS layer.<sup>44</sup> Moreover, the PCE can be further improved by treating various surface treatments.

## Conclusions

One-step electrodeposition method was employed to grow CIS thin films. The oxidation and reduction features related to Cu, In and Se were clearly observed in cyclic voltammetry. All reflections in XRD spectra are indexed to chalcopyrite crystal structure of CIS. Highly crystalline layers were grown after the post deposition heat-treatment in RTP. The average crystallite size calculated from the W-H analysis was in agreement with the values calculated from the Debye-Scherrer formula. SEM micrographs illustrate the granular grain growth of as-prepared layers which changes remarkably upon RTP annealing. The homogeneous and dense CIS layer with larger grain size about  $2\ \mu\text{m}$  was obtained after annealing. The energy band-gap value  $\sim 0.98\ \text{eV}$  was estimated for RTP annealed CIS layer which shows strong absorption in visible region. Raman study confirms the formation of pure chalcopyrite CIS phase, which is consistent with the corresponding XRD results. The Mott-Schottky and photo-electrochemical studies reveal the growth of p-type conductivity in all CIS layers. Electrical

**Table V.** Solar cell parameters obtained from selenized and RTP annealed CIS layers under dark and illuminated conditions.

Cell	$V_{oc}$ (V)	$J_{sc}$ ( $\text{mA}/\text{cm}^2$ )	FF	$\eta$ %	G (dark) ( $\text{mS}/\text{cm}^2$ )	G (ill) ( $\text{mS}/\text{cm}^2$ )	$R_s$ (dark) $\Omega\ \text{cm}^2$	$R_s$ (ill) $\Omega\ \text{cm}^2$
Glass/FTO/CdS/SelenizedCIS/Au	322	22	43	3.05	0.9	36	50.41	5.16
Glass/FTO/CdS/RTP annealed CIS/Au	364	32	51	5.94	0.4	7.5	23.40	4.31

measurements show the Schottky behavior for CIS layers. The ideality factor calculated for RTP annealed CIS layer close to unity due the highly crystalline layers with large grain growth. The atomic percentage concentrations obtained by EDAX analysis confirm the growth of stoichiometric CIS layers. The RTP process has the potential of improving electrical properties of the absorber layer by decreasing the amount of near surface defects. XPS studies confirms the presence of  $\text{Cu}^+$ ,  $\text{In}^{3+}$  and  $\text{Se}^{2-}$  oxidation states in as-prepared, selenized as well as RTP annealed CIS layers. Moreover, the composition obtained from XPS analysis for RTP annealed layer gives the formation of stoichiometric CIS formation. The device fabricated using selenized and RTP annealed CIS absorber layer gives the power conversion efficiency of 3.05% and 5.94%, respectively.

### Acknowledgment

The authors thank the Defense research and development organization (DRDO) under the major project grant (ERIP/ER/10003866/M/01/1388) and DST (SERI). ABR is thankful to CSIR for SRF fellowship No. 09/137/(558)/2015-EMR-I.

### References

- I. Khatri, H. Fukai, H. Yamaguchi, M. Sugiyama, and T. Nakada, *Sol. Energy Mater. Sol. Cells*, **155**, 280 (2016).
- A. N. Tiwari, D. K. Pandya, and K. L. Chopra, *Sol. Cells*, **22**, 263 (1987).
- M. A. Green, K. Emery, Y. Hishikawa, W. Warta, and E. D. Dunlop, *Prog. Photovolt. Res. Appl.*, **24**, 905 (2016).
- H. X. Zhang and R. J. Hong, *Ceramics International*, **42**, 14543 (2016).
- H. Lee, W. Lee, J. Kim, M. Ko, K. Kim, K. Seo, D. Lee, and H. Kim, *Electrochim. Acta*, **87**, 450 (2013).
- N. B. Chaure, J. Young, A. P. Samantilleke, and I. M. Dharmadasa, *Sol. Energy Mater. Solar Cells*, **81**, 125 (2004).
- R. N. Bhattacharya, J. F. Hiltner, W. Batchelor, M. A. Contreras, R. N. Noufi, and J. R. Sites, *Thin Solid Films*, **361-362**, 396 (2000).
- A. B. Rohom, P. U. Londhe, G. R. Bhand, M. G. Lakhe, and N. B. Chaure, *J. Mater. Sci. Mater. Electron*, **27**, 12374 (2016).
- P. U. Londhe, A. B. Rohom, and N. B. Chaure, *J. Mater. Sci. Mater. Electron*, **25**, 4643 (2014).
- H. S. Jadhava, R. S. Kalubaramea, S. Ahnb, J. H. Yunb, and C. Parka, *Appl. Surf. Sci.*, **268**, 391 (2013).
- P. U. Londhe, A. B. Rohom, and N. B. Chaure, *RSC Adv.*, **5**, 89635 (2015).
- N. B. Chaure, A. P. Samantilleke, R. P. Burton, J. Young, and I. M. Dharmadasa, *Thin Solid Films*, **472**, 212 (2005).
- A. R. Uhl, J. K. Katahara, and H. W. Hillhouse, *Energy Environ. Sci.*, **9**, 130 (2016).
- K. Ramanathan, F. S. Hasoon, S. Smith, D. L. Young, M. A. Contreras, P. K. Johnson, A. O. Pudov, and J. R. Sites, *J. of Phys. Chem. of Solids*, **64**, 1495 (2003).
- Z. Zhang, J. Li, M. Wang, M. Wei, G. Jiang, and C. Zhu, *Solid State Commun.*, **150**, 2346 (2010).
- H. Simchi, B. E. McCandless, K. Kim, J. H. Boyle, and W. N. Shafarman, *Thin Solid Films*, **535**, 102 (2013).
- A. M. Fernandez, M. E. Calixto, P. J. Sebastian, S. A. Gamboa, A. M. Hermann, and R. N. Noufi, *Sol. Energy Mater. Sol. Cells*, **52**, 423 (1998).
- N. G. Dhere, *Sol. Energy Mater. Sol. Cells*, **91**, 1376 (2007).
- N. B. Chaure, S. Bordas, A. P. Samantilleke, S. N. Chaure, J. Haigh, and I. M. Dharmadasa, *Thin Solid Films*, **437**, 10 (2003).
- M. E. Calixto, K. V. Dobson, B. E. McCandless, and R. W. Birkmire, *J. Electro. Chem.*, **153**, G521 (2006).
- S. De La Luz-Merino, M. E. Calixto, A. Mendez Blas, and B. Mari Soucase, *Mesoporous Biomater.*, **3**, 67 (2016).
- C. Sene, M. E. Calixto, K. V. Dobson, and R. W. Birkmire, *Thin Solid Films*, **516**, 2188 (2008).
- R. N. Bhattacharya, M. Oh, and Y. Kim, *Sol. Energy Mater. Solar Cells*, **98**, 198 (2012).
- A. J. Bard and L. R. Faulkner, Wiley, New York, 63 (2000).
- B. Scharifker and G. Hills, *Electrochim. Acta*, **28**, 879 (1983).
- S. K. Kulkurni, *Capital publishing Co.*, India (2007).
- B. D. Cullity and S. R. Stock, *NJ Prentice-Hall Inc., Englewood Cliff*, (2001).
- S. Nawale, V. Ravi, and I. S. Mulla, *Sens. Actuat. B*, **139**, 466 (2009).
- A. Chao, S. Ahn, J. H. Yun, J. G. Wak, S. K. Ahn, K. Shin, H. Song, and K. H. Yoon, *Sol. Energy Mater. Sol. Cells*, **109**, 17 (2013).
- J. H. Park and I. S. Yang, *Appl. Phys. A*, **58**, 125 (1994).
- O. Ramadani, J. F. Guillemoles, D. Lincot, P. PGrand, E. Chassaing, O. Kerrac, and E. Rzepka, *Thin Solid Films*, **515**, 5909 (2007).
- C. Rincon and C. Bellabarba, *Physical Review B*, **33**, 7160 (1986).
- C. C. Thompson, *Willard Grant Press*, (2007).
- F. Caballero-Briones, APalacios-Padrós, and F. Sanz, *Electrochim. Acta*, **56**, 9556 (2011).
- C. Guillen and J. Herrero, *Sol. Energy Mater. Sol. Cells*, **73**, 141 (2002).
- S. M. Sze and K. KNg, *Physics of Semiconductor Devices IIIrdedn.*, Wiley, New York, 170- (2007).
- E. A. Hernández-Pagán, W. Wang, and T. E. Mallouk, *ACS Nano*, **5**, 3237 (2011).
- S. Hamrouni, M. F. Boujmil, and K. Ben Saad, *Adv. Mater. Phys. Chem.*, **4**, 224 (2014).
- V. F. Lvovich, John Wiley & Sons, *INC., publication*, (2012).
- M. M. Shahid, A. Pandikumar, A. MGolsheikh, N. M. Huang, and H. N. Lim, *RSC Adv.*, **4**, 62793 (2014).
- J. Han, C. Liao, L. Cha, T. Jiang, H. Xie, K. Zhao, and M. P. Besland, *J. Phys. Chem. Solids*, **75**, 1279 (2014).
- B. Canava, J. Vigneron, A. Etcheberry, J. F. Guillemoles, and D. Lincot, *Appl. Surf. Sci.*, **202**, 8 (2002).
- S. SHegedus and W. N. Shafarman, *Prog. Photovolt. Res. Appl.*, **12**, 155 (2004).
- M. E. Calixto, K. V. Dobson, B. E. McCandless, and R. W. Birkmire, *Mater. Res. Soc. Symp. Proc.*, **865**, F14 (2005).